Applied Catalysis B: Environmental 90 (2009) 633–641

Contents lists available at ScienceDirect

Applied Catalysis B: Environmental

journal homepage: www.elsevier.com/locate/apcatb

Influence of sulfur on the structural, surface properties and photocatalytic activity of sulfated TiO_2

G. Colón [a,*], M.C. Hidalgo [a], J.A. Navío [a], A. Kubacka [b], M. Fernández-García [b]

[a] Instituto de Ciencia de Materiales de Sevilla, Centro Mixto Universidad de Sevilla-CSIC, Américo Vespucio s/n, 41092 Sevilla, Spain
[b] Instituto de Catálisis y Petroleoquímica, CSIC, C/Marie Curie 2, 28049 Madrid, Spain

ARTICLE INFO

Article history:
Received 27 February 2009
Received in revised form 20 April 2009
Accepted 25 April 2009
Available online 3 May 2009

Keywords:
Sulfated TiO_2 Photocatalyst
Defects
Microstrain
Raman
XPS
Phenol and toluene degradation

ABSTRACT

TiO_2 materials were prepared by sol–gel method and then impregnated with sulfuric acid and calcined using different temperatures and atmosphere (air and nitrogen). Systematic variation of these two experimental parameters makes possible to modulate the amount of surface sulfur from the impregnation procedure. The best photocatalyst for liquid phenol degradation was obtained after calcination at 700 °C in air, while gas toluene degradation optimum performance is obtained by calcination at 700 °C in nitrogen from 500 °C. Structural analysis of these materials by XRD, micro-Raman spectroscopy and FE-SEM shows that once calcined at 700 °C the material was a well-crystallized, high surface area anatase structure in all cases. The surface characterization by FTIR and XPS confirms the presence of a higher amount of sulfur species and acidic OH groups in samples partially calcined in nitrogen, and a low XPS O/Ti-atomic ratio with the O 1s peak shifted to higher binding energies (1.8 vs. 2 ± 0.1 and 530.4 eV vs. 529.8 eV, respectively, against the reference materials) for samples calcined at 700 °C, temperature at which most of sulfate species have been evolved. The paper presents an attempt to correlate the contribution of the observed structural defects within the anatase sub-surface layers and surface acidity to the different photoactivity behaviour exhibited for phenol liquid phase and toluene gas phase photodegradation.

1. Introduction

The improvement and optimisation of TiO_2 as a photocatalyst is an important task for technical applications of heterogeneous photocatalysis in the future. In this sense, many investigations on the basic principles and enhancement of the photocatalytic activity either in the ultraviolet or visible have been carried out [1,2]. The activity of a TiO_2 powder depends on its bulk and surface properties. Regarding to the surface properties, the enhancement of acidity of the semiconductor is reported as a feasible way to enhance the photocatalytic activity of TiO_2. It is well known that WO_3 or MoO_3 increases the surface acid properties of TiO_2 improving at the same time the UV-photon efficiency by increasing the adsorption of the pollutant [3,4]. Incorporation of W^{6+}, up to ca. 20%, into the bulk of the anatase lattice promotes photoactivity in the visible due to generation of cation vacancies [5,6].

Moreover, the improvement of the final photocatalytic properties might be achieved by influencing those properties which control either the charge carrier dynamics (carrier generation, transfer and diffusion) or the surface catalytic process, which are the quality of the structure and the surface features.

It has been widely reported that sulfated TiO_2 could have interesting photocatalytic properties in certain reactions [7–9]. The improved efficiency of the sulfated materials might be due to a greater surface area as well as the larger fraction of anatase phase. However a combination of both effects, the increase of acid properties and the larger surface area with an appropriate structure cannot be excluded in principle. Deng et al. [10] concluded that the improved photocatalytic activity of sulfated TiO_2 should be grounded in a combining effect of the presence of sulfate on the catalyst surface and the increase in catalyst surface area. However, no significant effect of sulfation was found for sulfated rutile TiO_2. In this sense, previous works pointed out that acid treated TiO_2 might present an oxygen defective surface [11]. Therefore, it may be expected that sulfation pretreatment clearly leads to an oxygen deficient surface [12,13]. We concluded that anatase stabilization by sulfate ions up to 700 °C and the creation of bulk oxygen vacancies through a dehydroxylation process of the excess of adsorbed protons seems to be responsible for the generation of a highly defective material. The loss of the oxide ions from their surface and the small fraction of rutile phase would lead to clear enhancement in the UV-photocatalytic activity of these materials by the improvement of the charge separation and

* Corresponding author.
E-mail addresses: gcolon@icmse.csic.es (G. Colón), mfg@icp.csic.es (M. Fernández-García).

0926-3373/$ – see front matter © 2009 Elsevier B.V. All rights reserved.
doi:10.1016/j.apcatb.2009.04.026

diffusion to the surface. Recently Rengifo-Herrera et al. have shown that N and S co-doped materials showed suitable photocatalytic activity under UV and visible illumination towards *Escherichia coli* inactivation [14]. They also argued that catalysts showed a varying degree of hydroxylation and particles sizes affecting to the trapping and transfer of the charge carriers and therefore to the semiconductor performance.

It is well known that sulfate groups are stable in the oxide structure during calcination up to 600 °C [15,16]. Indeed, we reported that the DTG curve of the sulfated TiO_2 showed a weight loss between 400 and 600 °C that could be due to the decomposition of strongly bonded sulfate species. The disappearance of surface sulfate would take place in three well-defined steps denoting the existence a three sulfate families probably with different acid strength [12,13]. In the present paper we have obtained different presulfated TiO_2 systems with tuned amount of residual surface sulfates which would allow tailoring the structural and surface feature of the catalysts. The residual surface sulfate was stabilized by changing the calcination atmosphere from air to nitrogen at two different temperatures. This way we assure the occurrence of a different surface situation in the final TiO_2 photocatalyst.

2. Experimental

As previously reported [12], TiO_2 was prepared by a sol–gel method using titanium tetraisopropoxide (TIP) as precursor in isopropanol (3.9 ml TIP in 200 ml iPrOH). Hydrolysis of the isopropanol-TIP solution was achieved by adding certain volume of bidistilled water (TTIP:H_2O = 0.05). The precipitate was then filtered and dried at 120 °C overnight and divided in two portions. Sulfation of one of the batch was performed by dispersing the fresh dried powders in a H_2SO_4 1 M solution (50 ml/g) for 1 h. Then, the suspension was filtered off and the powder dried again at 120 °C overnight. Sulfated TiO_2 samples (hereafter, TS series) were calcined in flowing air at 650 and 700 °C for 2 h. Air flow was changed to N_2 atmosphere at different temperature (T_c = 500 and 600 °C) labelled hereafter by adding a number to the series label that indicates the temperature of calcination and the T_c temperature (i.e. TS650_Tc500 will mean samples calcined at 650 °C with N_2 atmosphere changing temperature at 500 °C). The thermal programme used in the calcinations is presented in Fig. 1.

BET surface area and porosity measurements were carried out by N_2 adsorption at 77 K using a Micromeritics 2000 instrument.

FTIR spectra were acquired using the transmission mode upon pellets of the studied powdered samples dispersed in KBr, using a Nicolet spectrometer (20SXB) with a DTGS detector, in the range of 4000–400 cm^{-1} with a resolution of 4 cm^{-1}. The samples were uniformly ground in an agate mortar with KBr previously degasified at 400 °C.

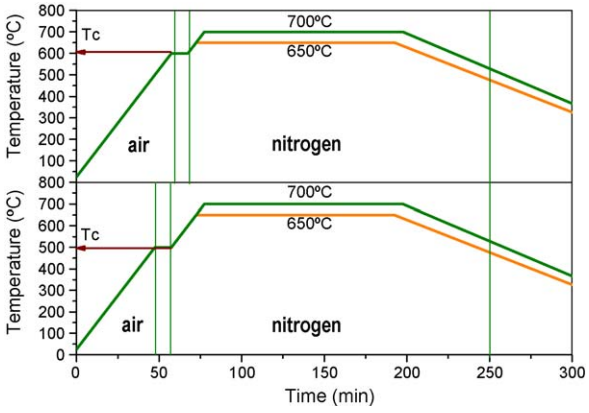

Fig. 1. Representation of the thermal programmes used.

X-ray diffraction (XRD) patterns were obtained using a Siemens D-501 diffractometer with Ni filter and graphite monochromator. The X-ray source was Cu Kα radiation (0.15406 nm). The line broadening (β_{hkl}) of X-ray diffraction peak corresponding to anatase phase planes was determined by deconvolution of the corresponding peak using a Voigt function. These values were incorporated into Williamson–Hall equation [17] for each sample according to the following expression:

$$\frac{\beta_{hkl}\cos\theta_{hkl}}{\lambda} = \frac{4\varepsilon\sin\theta_{hkl}}{\lambda} + \frac{1}{d}$$

where ε is the microstrain, d the crystallite size, λ the wavelength of the X-ray radiation 0.15406 nm and θ_{hkl} the diffracting angle.

Micro-Raman measurements were performed using a LabRAM Jobin Yvon spectrometer equipped with a microscope. Laser radiation (λ = 532 nm) was used as excitation source at 5 mW. All measurements were recorded under the same conditions (1 s of integration time and 30 accumulations) using a 100× magnification objective and a 125 μm pinhole.

The morphology of TS samples was followed by means of field emission-SEM (Hitachi S 4800). The samples were dispersed in ethanol using an ultrasonicator and dropped on a copper grid.

UV–vis spectra were recorded in the diffuse reflectance mode (R) and transformed to a magnitude proportional to the extinction coefficient (K) through the Kubelka–Munk function, $F(R_\infty)$. Samples were mixed with $BaSO_4$ that does not absorb in the UV–vis radiation range (white standard). Scans range was 240–800 nm.

XPS data were recorded on 4 mm × 4 mm pellets, 0.5 mm thick, prepared by slightly pressing the powdered materials which were outgassed in the prechamber of the instrument at 150 °C up to a pressure $< 2 \times 10^{-8}$ Torr to remove chemisorbed water from their surfaces. The Leibold-Heraeus LHS10 spectrometer main chamber, working at a pressure $< 2 \times 10^{-9}$ Torr, was equipped with an EA-200 MCD hemispherical electron analyzer with a dual X-ray source working with Al Kα ($h\nu$ = 1486.6 eV) at 120 W, 30 mA using C(1s) as energy reference (284.6 eV). Surface chemical compositions were estimated from XP-spectra, by calculating the integral of each peak after subtraction of the "*S-shaped*" Shirley-type background using the appropriate experimental sensitivity factors [18].

Photocatalytic runs (2 h) of phenol oxidation using different catalysts (1 g/l) were performed in a batch reactor (250 ml) using a Osram Ultra-Vitalux lamp (300 W) with sunlike radiation spectrum and a main line in the UVA range at 365 nm. The intensity of the incident UVA light on the solution was measured with a PMA 2200 UVA photometer (Solar Light Co.) being ca. 105 W/m^2. In the oxidation tests, an oxygen flow was employed what produces a homogenous suspension of the catalyst in the solution. Before each experiment, the catalysts were settled in suspension with the reagent mixture for 15 min. The evolution of the initial phenol concentration (ca. 50 ppm) was followed through the evolution of the characteristic 270 nm band using a filtered aliquot ca. 2 ml of the suspension (Millipore Millex25 0.45 μm membrane filter). Total organic carbon was followed by means of a TOC analyzer (Shimadzu TOC VCPH).

Activity and selectivity for the gas phase photooxidation of toluene were tested in a continuous flow annular photoreactor (described elsewhere, Ref. [19]). The corresponding amount of catalyst was suspended in 1 ml of water, painted on a pyrex tube (cut-off at ca. 290 nm) and dried at RT. Thus, ca. 30 mg of photocatalyst is disposed as a thin layer coating on the pyrex tube showing an irregular thickness of ca. 40 μm. In any case, the reaction rates measured and reported were independent of the film thickness in the 20–60 μm range. The reacting mixture (100 ml/min) was prepared by injecting toluene (Panreac, spectroscopic grade) into a

wet (ca. 75% relative humidity, RH) 20 vol.% O_2/N_2 flow before entering at room temperature to the photoreactor, yielding an organic inlet concentration of ca. 800 ppmv. Under such conditions, the reaction rate shows a zero order kinetic following a Langmuir–Hinshelwood mechanism with respect to the total flow and hydrocarbon/oxygen concentrations. After flowing the mixture for 1 h (control test) in the dark, the catalyst was irradiated by four fluorescent daylight lamps (6 W, Sylvania F6W/D) with a radiation spectrum simulating sunlight (UV content of 3%), symmetrically positioned outside the photoreactor. Reference experiments with UV lamps (Sylvania F6WBLT-65; 6 W, max. at ca. 350 nm) were run using the same reaction set-up and procedure. Reaction rates were evaluated (vide supra) under steady state conditions, typically achieved after 3–4 h from the irradiation starting. No change in activity was detected for all samples within the next 6 h. The concentration of reactants and products was analyzed using an on-line gas chromatograph (HP G1800C) equipped with a HP5 capillary column (0.25 mm I.D. × 30 m) and a flame ionization detector using a SIM mode.

3. Results and discussions

Main structural characterization data for the materials used in this work throughout the thermal evolution of the precursor have been summarized in Table 1. All sulfated TiO_2 samples exhibit relatively high surface areas with respect to the non-sulfated ones calcined at such high temperature (see Ref. [13]). Indeed, the presence of sulfate at the surface stabilizes the surface area values, as it has been widely accepted. Thus, after the calcination at 650 and 700 °C the specific surface area presents a rather high value of 45 and 24 m^2/g, respectively. The similar thermal treatment under inert atmosphere slightly affects this reference value independently of the T_c temperature. Thus, it appears that calcination under N_2 produces a certain stabilization of the surface area, especially for samples calcined at 650 °C.

In Fig. 2 we show the progress of the pore diameter for sulfated samples calcined at 650 and 700 °C. It can be observed that sample calcined at 650 °C (ST_650) present a bimodal pore distribution, with two plain pore families at 75 and 110 nm. The sample calcined at 700 °C (ST_700) in air only exhibits a narrow pore size distribution located at 125 nm. Thus, during the calcination in air, as temperature increases from 650 to 700 °C, the mean pore size develops from 75 to >120 nm. Such evolution of the pore size with the calcination temperature was already reported by some of us [12]. From this figure it is clear that initial mean pore size of TiO_2 precursor was stabilized by the presence of surface sulfates. As these sulfates are eliminated by calcination in air, it is observed the progressive shift in the average pore size. For the series calcined at 650 °C, the calcination in nitrogen produces a narrow pore size distribution located at 65–70 nm. The calcination following this combined regimes ($O_2 + N_2$) leads to the disappearance of the higher size pore family (>120 nm) resulting in a final monomodal pore size distribution. It also

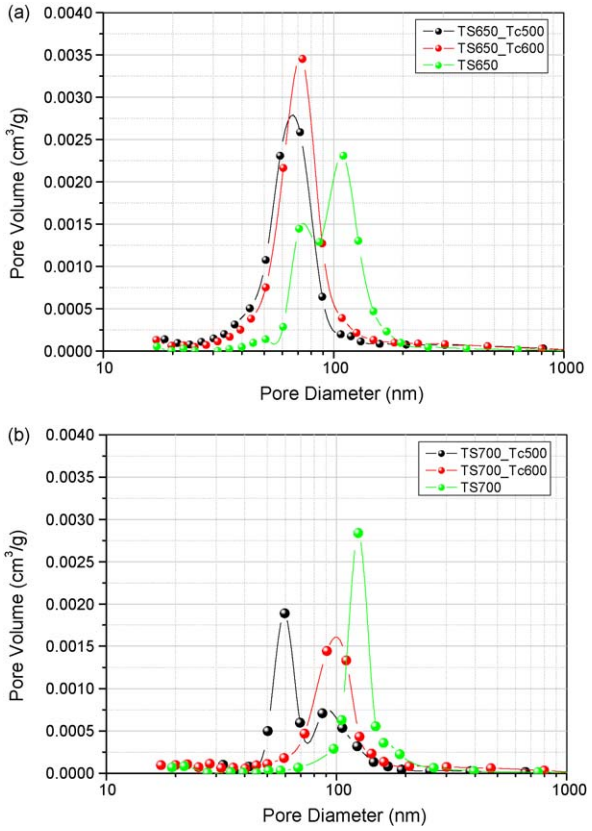

Fig. 2. Evolution of the pore diameter for (a) TS650 series and (b) TS700 series.

appears that a small shift can be detected in the mean pore size as T_c increases (from 65 to 70 nm). In this case, as sulfur vestiges at the surface should be slightly lower for T_c = 600 °C with respect to T_c = 500 °C, the mean pore size shifted towards higher values. From DTG curves it was reported that different families of sulfates can be described [12,13]. After calcination at 650 °C, probably a residual portion of the most strongly linked sulfates remains. We may infer that the decomposition of such surface sulfates induces a certain development of porosity of higher diameter. When calcination is performed in nitrogen this progression is delayed due to the stabilization of these sulfates at the surface.

Regarding to the series calcined at 700 °C, the calcination in nitrogen clearly shows that this transition in the pore size distribution is already starting for T_c = 500 °C sample. By increasing the T_c temperature at 600 °C, the pore distribution becomes monomodal with a mean pore size of 100 nm. Subsequently, at 700 °C the residual sulfates remaining after changing to nitrogen at T_c = 500 °C produces a certain stabilization of the initial pore structure. When nitrogen is introduced at 600 °C the remaining

Table 1
Surface and structural properties of TS photocatalysts.

Photocatalyst	S_{BET}, m^2/g	Anatase fraction, %	Crystalline size, nm[a]	Crystalline size, nm[b]	Microstrain, $\times 10^{4}$[b]	Band gap, eV
TS650_Tc500	47 ± 3	100	15 ± 1	21 ± 2.0	24.3 ± 2.1	3.14
TS650_Tc600	55 ± 3	100	14 ± 1	18 ± 1.5	19.2 ± 2.0	3.17
TS650	45 ± 3	100	17 ± 1	19 ± 1.5	7.9 ± 0.8	3.14
TS700_Tc500	20 ± 1	100	27 ± 2	33 ± 3.1	8.0 ± 0.8	3.16
TS700_Tc600	31 ± 2	100	27 ± 2	32 ± 3.0	9.0 ± 1.0	3.17
TS700	24 ± 1	100	28 ± 2	30 ± 3.0	2.4 ± 0.2	3.16

[a] Anatase crystallite size calculated from XRD peak broadening using Scherrer equation.
[b] Anatase crystallite size and microstrain calculated from XRD peak broadening using Williamson–Hall method.

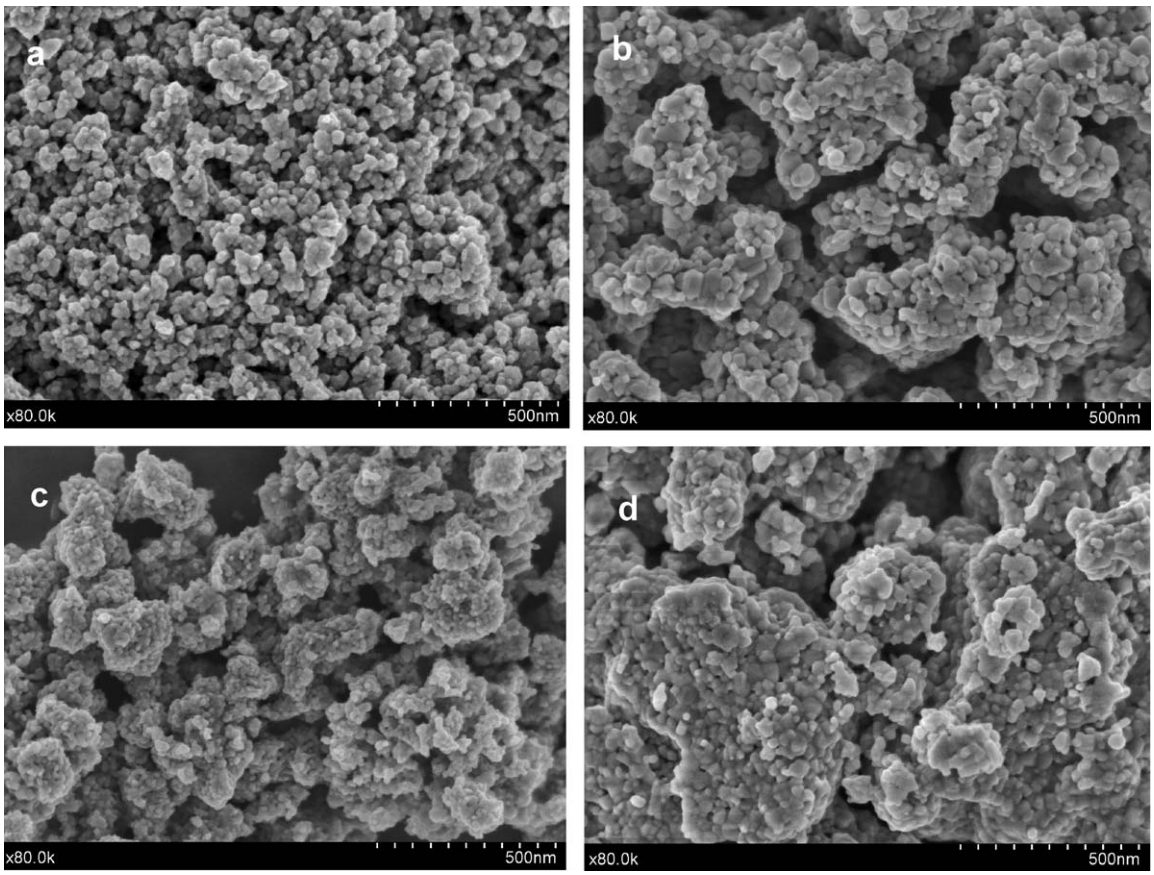

Fig. 3. SEM images for (a) TS650, (b) TS700, (c) TS650_Tc500 and (d) TS700_Tc500 samples.

amount sulfate is not able to stabilize the pore structure after calcination at 700 °C.

The evolution of the XRD for sulfated series calcined at 650 and 700 °C under different conditions shows clearly that only anatase crystalline phase is present (Table 1). Moreover, no peaks corresponding to brookite, rutile or sulfate species are present in samples calcined in air or N_2. It can be seen that sulfate loading of the fresh precursor stabilizes a well-crystallized pure anatase phase upon isothermal calcination even at 700 °C. This fact has been already pointed out in our previous paper in which we concluded that the phase transition in our sulfated precursor took place either at temperatures >700 °C or for longer heating times at this temperature [12,13]. Thus, the presence of sulfate shifts the anatase to rutile transition in the case of the sulfated TiO_2 precursor towards higher temperature with respect to non-sulfated one. The calculated crystallite sizes for samples calcined at 650 and 700 °C are, respectively, 17 and 28 nm. For the samples calcined at 650 °C in N_2, it can be pointed out a small decrease in the crystallite size, being this diminution negligible for those similarly calcined at 700 °C. In fact the presence of residual sulfates upon calcination in N_2 would retard the crystallization in a small extent. Such delay appears minor for calcination at 700 °C. From the Williamson–Hall plot it has been obtained the microstrain values for all samples (Table 1). As expected, the samples calcined at 650 °C show higher microstrain values with respect to the series calcined at 700 °C. The lowest value within the series corresponds to the sample calcined in air. Thus, it can be inferred that the calcination in nitrogen induces a slight degree of surface strain associated to the existence of the sulfate residue. Concerning to the series calcined at 700 °C, the calculated microstrain for samples calcined in nitrogen after different T_c temperature present almost the same value, indicating that the different T_c temperature does not represent a conditioning parameter at 700 °C. However, and similarly to the 650 °C series, the calcination in air present the best structural situation at this temperature.

The morphology of selected samples has been analyzed in Fig. 3. In both series, small and homogenous roundish shaped particles can be found. The observed particle sizes for TS650 and TS700 samples (Fig. 3a and b) appear significantly different (ca. 15–20 and 30–40 nm, respectively) and are in good accordance to the crystallite size calculated from XRD (Table 1). Samples partially calcined in nitrogen (Fig. 3c and d) show a clear different morphology. Thus, calcination in nitrogen produces a lower defined agglomeration of particles indicating a lower crystallization degree. This is a clear evidence of the surface ad structural stabilization of sulfate rest against sintering.

In Fig. 4, we show the FTIR spectra of sulfated TiO_2 samples in the range 4000–2500 cm^{-1}. Within this range it shows up the bands corresponding to surface hydroxyl groups. Two clear bands can be observed in both series, one located at 3400 cm^{-1} and a second one located around 3100 cm^{-1}. These bands can be attributed to the different OH groups at the surface. As expected, the bands come up with lower intensity in samples calcined at 700 °C denoting the loss of hydroxylation due to calcination. For samples calcined at 650 °C in nitrogen the IR spectra do not differ with the T_c temperature, but it is worth of noting a more prominent contribution of the 3100 cm^{-1} band with respect to the sample calcined in air. This would indicate that this band might be associated to more acidic hydroxyl groups related to the existence of surface sulfates. The calcination at 700 °C seems to minimise such differences between samples calcined in air and nitrogen. In

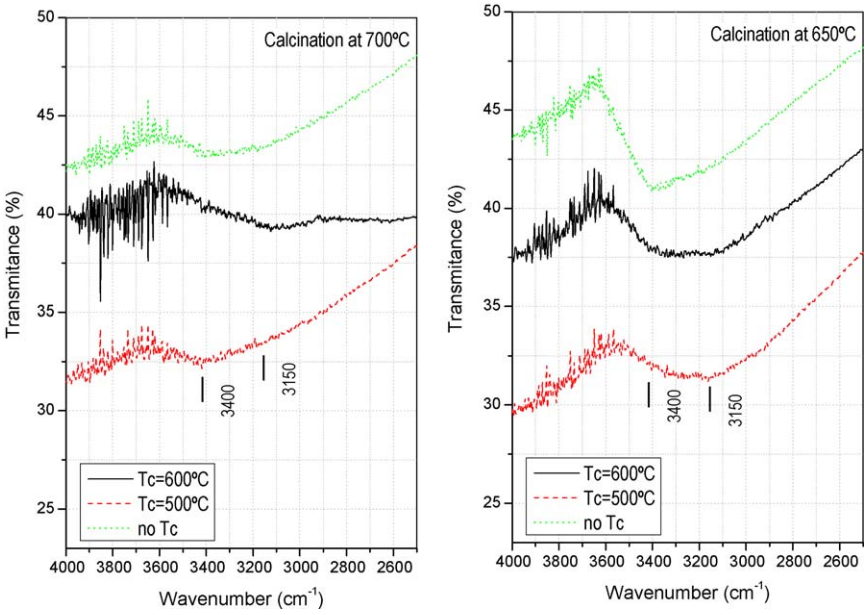

Fig. 4. FTIR spectra for TS650 series and TS700 series in the range 4000–2500 cm^{-1}.

all cases within this series a rather dehydroxylated surface would be inferred without any influence of the T_c temperature.

Considering the range between 1800 and 400 cm^{-1} we may attend the bands corresponding to sulfate species at the surface (Fig. 5). The peaks at 1265, 1130 and 1040 cm^{-1} were the characteristic frequencies of a bidentate SO_4^{2-} co-ordinated to metals such as Ti^{4+} [20]. Those peaks are observable in Tc500 samples calcined at 650 and 700 °C, indicating that the partial calcination in nitrogen from this T_c temperature would preserve to certain extent the surface sulfate from the starting sulfated TiO_2 precursor. When sample is calcined at 650 °C, it is also possible to detect small sulfate bands in Tc600 sample since this calcination temperature is not sufficient for the elimination of sulfates. However, the calcination at 700 °C leads to an almost sulfate free surface for Tc600 sample and indeed for the sample calcined in air. Those results clearly indicate the possibility of tuning the remaining sulfates on the TiO_2 surface by changing the calcination temperature and atmosphere.

The evolution of the different sulfated TiO_2 has been also followed by Raman spectroscopy. As shown in Fig. 6, from the irreducible presentation of the optical modes it is possible to distinguish the three TiO_2 polymorphs by means of Raman spectroscopy [21]. Thus, the anatase crystal phase shows 6 active modes: 150 (E_g), 196 (E_g), 396 (A_{1g}/B_{1g}), 516 (A_{1g}) and 640 cm^{-1} (E_g). From the observation of the Raman spectra in Fig. 6, it is possible to infer that the anatase phase is the predominant one in both series. In addition, for series of samples calcined at 650 °C it is possible to detect small bands at 247 and 322 cm^{-1} that might be associated to the brookite phase. These bands almost disappeared for the series calcined at 700 °C which only exhibits a small broad shoulder at around 320 cm^{-1}. This small contribution in samples calcined at 700 °C would also be associated with the creation of a

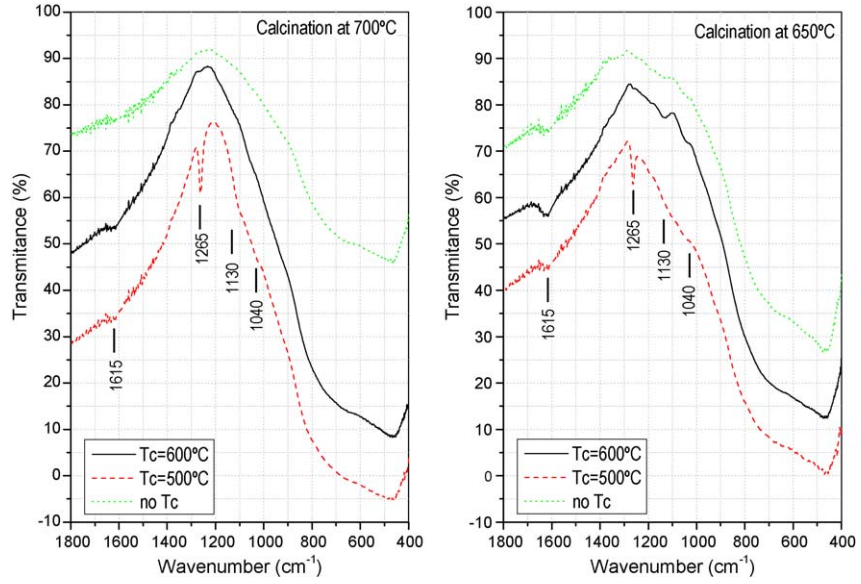

Fig. 5. FTIR spectra for TS650 series and TS700 series in the range 1800–400 cm^{-1}.

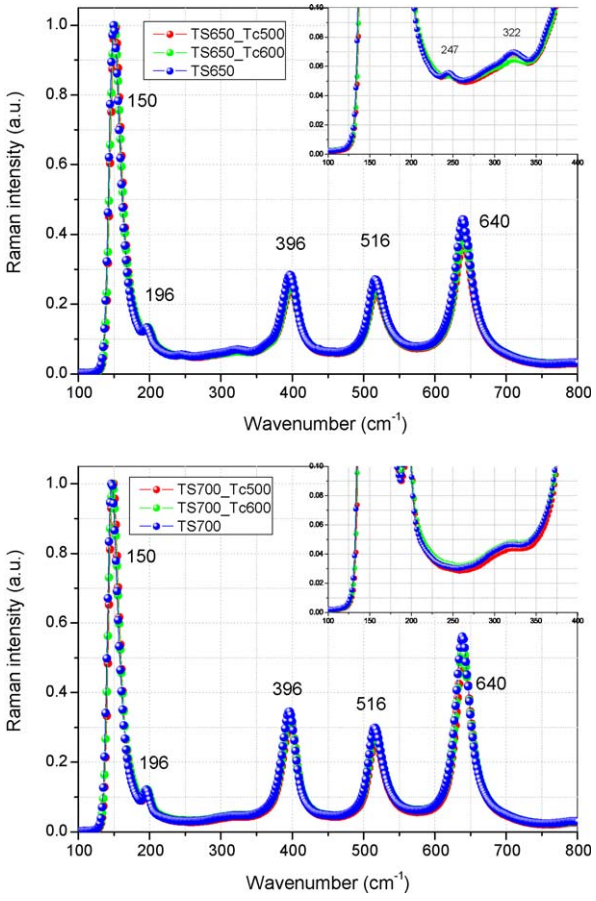

Fig. 6. Raman spectra for TS650 series and TS700 series.

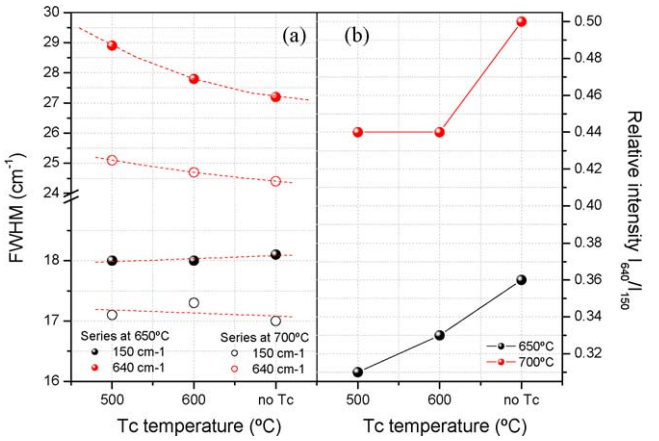

Fig. 7. Evolution of (a) FWHM for E_g bands at 150 and 640 cm^{-1} and (b) the relative intensity for E_g band at 640 cm^{-1} with respect to band at 150 cm^{-1}.

fraction of a metastable structure derived from the elimination of the surface sulfate that could indicate a certain transition stage between brookite and anatase. As we have previously reported, the last stage of sulfate elimination would produce a certain amount of oxygen deficiencies originated from the sulfate evolving process. This observation is in agreement with the microstrain data discussed above.

Another feature that can be pointed out concerns to the small variations detected in the position of the anatase E_g band located at around 150 cm^{-1} (Table 2). This shift in the position of the Raman lower energy E_g band (vibrational mode v5, assigned to the Ti/O bond stretching type vibrations) and the broadening in the FWHM of such band have been widely reported. In this sense, the interpretations about the variations of Raman peak shape involve pressure effect due to the surface tension of grains [22,23], nonstoichiometry such as oxygen deficiency or disorder induced by some minor phases in the sample [24] and phonon confinement effects with the grain size variation [25]. In Table 2, we have reported the Raman shift values and FWHM for all bands corresponding to both sulfated TiO_2 series. As well known, band position shifts are always difficult to analyze due to their limited size in comparison with experimental error; [26] however a decreasing trend in both TS650 and TS700 series is observed in Table 2. More informative is the analysis of the band intensity. In particular, it is possible to observe that the relative intensity (I_{640}/I_{150}) suffers a significant decrease for series calcined at 650 °C with respect to those for 700 °C series (Fig. 7). The lower relative intensity calculated for 650 °C (0.31–0.36) indicate that the surface sulfate would affect to this vibrational mode associated to the Ti/O stretching [27]. The presence of these residual sulfates at the surface seems to affect the lattice vibration diminishing the band intensity at ca. 640 cm^{-1}. Indeed, within this series, as T_c temperature increases and fewer sulfates are present, the relative intensity slightly grows up. For samples calcined at 700 °C the intensity for band at 640 cm^{-1} appears with a relative intensity higher than 0.44, being for the sample calcined in air (TS700) 0.5. That means that for this series the small amount of sulfate residue produces a increase in the band intensity. At the same time, if we observe the evolution of the FWHM for E_g bands at 150 and 640 cm^{-1}, an interesting behaviour can be inferred. Concerning the band at 150 cm^{-1}, no significant change in the FWHM is observed for the different calcination treatments. On the contrary, the FWHM for the 640 cm^{-1} band seems to decay as T_c temperature increases being more evident for samples calcined at 650 °C. Therefore it can be deduced a direct relationship between the residual sulfates and the band shape/width. Since the difference in crystallite sizes within TS650 or TS700 individual series is not significant, we may suppose that the FWHM decrease within each series could be associated to a decreasing presence of defects (and/or surface strain derived from the presence of alien sulfate surface species).

Table 2
Raman shift and FWHM values for anatase bands.

Photocatalyst	E_g (cm^{-1})		B_{1g} (cm^{-1})		$A_{1g} + E_g$ (cm^{-1})		E_g (cm^{-1})	
	Centre	FWHM	Centre	FWHM	Centre	FWHM	Centre	FWHM
TS650_Tc500	154.9	18.0 ± 2	397.8	25.9 ± 3	518.6	28.2 ± 3	640.5	28.9 ± 3
TS650_Tc600	154.4	18.0 ± 2	397.5	25.1 ± 3	518.6	26.8 ± 3	640.5	27.8 ± 3
TS650	153.3	18.1 ± 2	396.8	24.4 ± 3	517.7	26.9 ± 3	639.6	27.2 ± 3
TS700_Tc500	152.4	17.1 ± 2	396.4	24.1 ± 3	517.9	25.0 ± 3	640.2	25.1 ± 3
TS700_Tc600	151.9	17.3 ± 2	395.8	23.9 ± 3	517.3	24.7 ± 3	639.5	24.7 ± 3
TS700	150.8	17.0 ± 2	395.1	23.4 ± 3	516.8	24.7 ± 3	638.9	24.4 ± 3

Table 3
Surface chemical analysis from XPS for TS photocatalysts calcined at different temperatures.

Photocatalyst	Atomic%		O/Ti	S/Ti ($\pm 3 \times 10^{-3}$)
	S	C		
TS650_Tc500	1.01	4.64	1.95 ± 0.15	0.031
TS650_Tc600	0.99	6.50	2.00 ± 0.15	0.033
TS650	1.00	1.87	1.88 ± 0.15	0.031
TS700_Tc500	0.82	5.10	2.03 ± 0.15	0.026
TS700_Tc600	0.65	2.40	1.82 ± 0.15	0.018
TS700	0.70	3.10	1.87 ± 0.15	0.024

From the UV–vis spectra (not shown) for TS series we have calculated the band gap values (Table 1). These values appear similar for all samples from 3.14 to 3.17 eV. The small differences observed are within the experimental error (±0.1 eV).

The study of the surface composition has been performed by means of XPS analysis. In Table 3 we show the sulfur and carbon surface contents for the studied samples. Two important features can be observed from these data. Firstly similar sulfur content is obtained within the series of samples calcined at 650 °C leading to S/Ti ratio of around 0.032. For the series of catalysts calcined at 700 °C the S/Ti ratio lay down to ca. 0.020. Related to this value, the O/Ti ratio denotes the existence of oxygen deficient surface structure especially in the case of samples calcined in air. As we previously reported [13], the elimination of surface sulfates leads to the creation of oxygen vacancies in a sublayer position. Thus, the sub-stoichiometric situation for samples calcined in air is explained by considering the proposed surface mechanism during thermal treatment. In Table 4, we show the binding energy values for Ti 2p, O 1s and S 2p electronic levels. It is worthy to note that the Ti 2p energy values shift slightly in all cases towards higher values with respect to the reference TiO_2 [13], indicating a very strong interaction between the sulfate anion and titanium cation with increased positive polarity. Such an interaction has also been reported by Anderson and co-workers [28]. The same effect is observed for the O 1s contribution associated to TiO_2 lattice oxygen, with averaged binding energies higher than 530 eV in all cases. In addition, for samples partially calcined in nitrogen with T_c = 500, additional contributions can be detected in the O 1s XPS spectrum (Fig. 8a). These additional bands at ca. 532 and 533 eV could be related to the different hydroxyl groups at the surface. In fact, from FTIR spectra it was denoted that new band at around 3100 cm^{-1} arises for sulfated samples calcined in nitrogen. Thus, it could be assumed that certain hydroxyl groups can be located in the vicinities of surface sulfates leading to this new contribution at ca. 533 eV. Furthermore, the existence of such OH is also observed for the two samples calcined at 650 °C in nitrogen (Table 4). Regarding to S 2p spectra (Fig. 8b) the deconvolution analysis shows one kind of oxidized sulfur species in all the surfaces, characterized by a single S 2p doublet at ca. 168.5 and 169 eV. This signal could be ascribed to Ti^{4+} coordinated SO_4^{2-} species. In the case of samples calcined in nitrogen with T_c = 500 °C the B.E. for S 2p band is located at 0.5 eV higher energy. This significant shift to higher energy denotes a different environment surrounding the sulfur ions with considerable positive polarity. Such significant shift can be tentatively explained by considering the above proposed oxygen defects in the sublayer position which could produce a noticeable electron extra drain from S^{6+} ions.

Table 4
Binding energies from XPS for TS photocatalysts calcined at different temperatures.

Photocatalyst	Ti 2p	O $1s_I$	O $1s_{II}$	O $1s_{III}$	S 2p
TS650_Tc500	459.3	530.6	532.2	533.3	169.3
TS650_Tc600	459.1	530.7	532.3	533.1	168.8
TS650	459.5	531.3	532.8	–	168.5
TS700_Tc500	459.4	530.6	532.1	533.2	169.6
TS700_Tc600	459.1	531.1	532.5	–	169.0
TS700	459.0	530.2	531.5	–	169.0

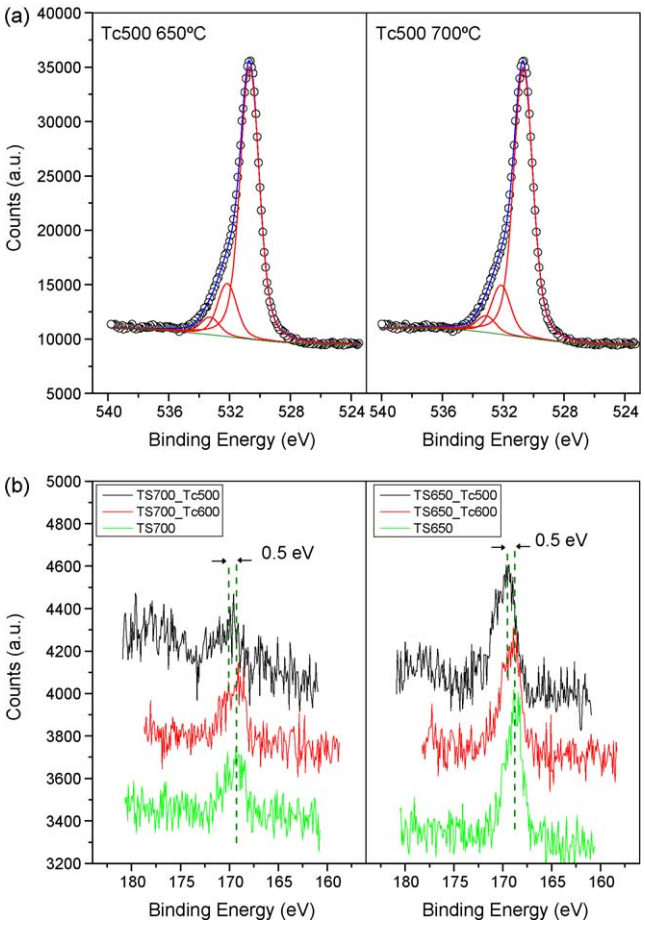

Fig. 8. XPS spectra for (a) O 1s and (b) S 2p for selected TS samples.

The photocatalytic activity of TS series was studied using the photo-oxidation of phenol tests under UV-irradiation. Conversion curves are plot in Fig. 9. Series calcined at 650 °C exhibit similar behaviour for the phenol degradation reaction with conversion rates around 5×10^{-8} mol/l s. The TOC at the end of the reaction appear in all cases at around 15%, indicating a good agreement with phenol disappearance evolution. Different calcination treatments do not induce significant changes in the photocatalytic performance of the catalysts. The reaction rates for series calcined at 700 °C present higher values with respect to 650 °C series. In this case, samples calcined at 700 °C show a clear evolution depending on the thermal treatment. From the reaction rate values it is possible to infer that the increasing sulfate residue leads to a progressive decrease in the phenol degradation rate (Fig. 10a). TOC evolution within this series also indicates good agreement with phenol concentration. Final TOC for these samples appeared around 8% in all cases. Thus, the higher photoactivity is found for sample calcined at 700 °C in air, for which a lower sulfur content and optimal structural situation have been described above. Therefore, the presence of a certain sulfate rest at the surface would negatively affect to the phenol degradation by either blocking the active sites and/or avoiding the formation of new

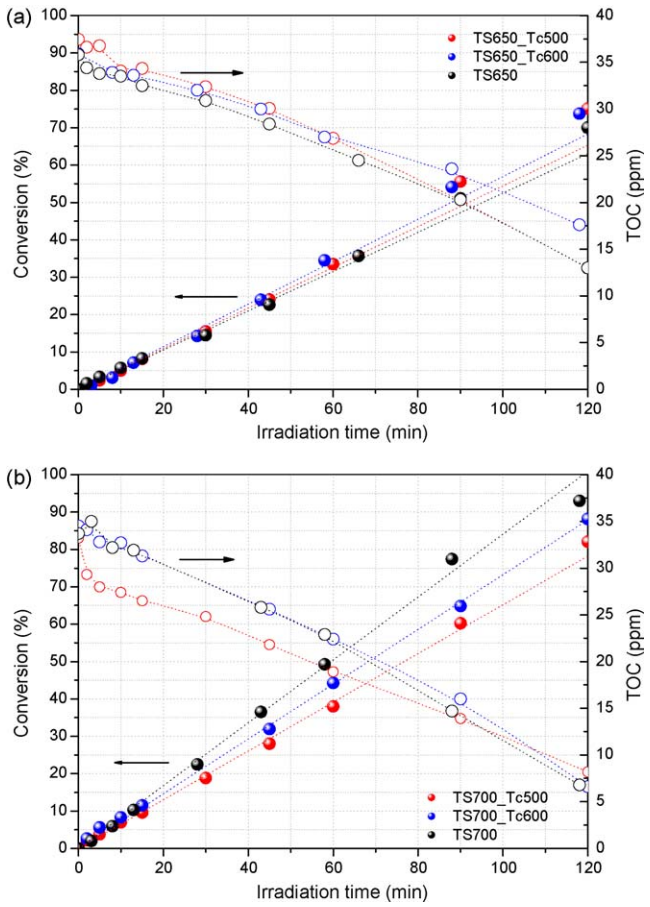

Fig. 9. Evolution of phenol concentration and TOC during photocatalytic reaction for (a) TS650 series and (b) TS700 series.

highly active sites. In fact we have previously suggested that a defective surface structure would result after the elimination of surface sulfates during calcinations [13]. These sublayer oxygen defective sites, formed after the elimination of sulfates, would also promote the formation of a small rutile seeds in the vicinities of the oxygen vacancies. We have proposed that such particular structure would be responsible of the enhanced photoactivity for phenol degradation.

Regarding to the toluene photooxidation reaction (Fig. 10b), reaction rates for series calcined at 650 and 700 °C show similar evolutions with the thermal treatment. The increasing T_c temperature clearly leads a progressive decrease in the photocatalytic activity. Furthermore, the samples calcined in air (no T_c samples) present the lower activity for toluene degradation. In this sense it can be pointed out that as sulfur content diminishes the photoactivity decays. As Barraud et al. reported the presence of small amount of surface sulfates positively affects the photoactivity in this particular reaction [29]. The partial calcination in nitrogen at such high temperatures stabilizes a certain residue of sulfates at the surface. This small amount would assure the photoactivity of our systems since higher sulfate content seems to be not beneficial for toluene photodegradation [7]. At the same time, the structural, morphological, and surface (particularly surface acidity as deduced from the IR study) features are optimised due to the thermal treatment and the presence of the above mentioned sulfate residue. The presence of sulfates also affect selectivity, as the selectivity to total oxidation decreases nearly a 25% from samples calcined in air to those having the larger sulfate content (Tc500 samples).

There generally exist two proposed reaction mechanisms for the photogenerated holes on TiO_2 photocatalyst: (i) the holes react with surface hydroxyl groups to produce highly active hydroxyl radicals which initiate photo-oxidation reactions [30,31] and (ii) the holes are directly trapped by chemisorbed organic molecules [32,33,23]. Despite the disagreements on the reaction pathways of photogenerated holes, it can be assumed that the high density of surface hydroxyl groups was helpful for both •OH-driven and direct hole oxidation pathways. In our case the occurrence of well-crystallized anatase structure with certain amount of oxygen defects that could participate in the diffusion mechanism of charge carrier do enhance the photoactivity for phenol degradation in liquid phase. Furthermore, it has been demonstrated that the existence of sulfur residue clearly produces a detriment in the photocatalytic activity. On the other hand, the above mentioned features seem to benefit the toluene degradation in the gas phase. Thus, the presence of acidic OH groups due to the small sulfur residue appears as a key point for the photoactivity improvement in this reaction.

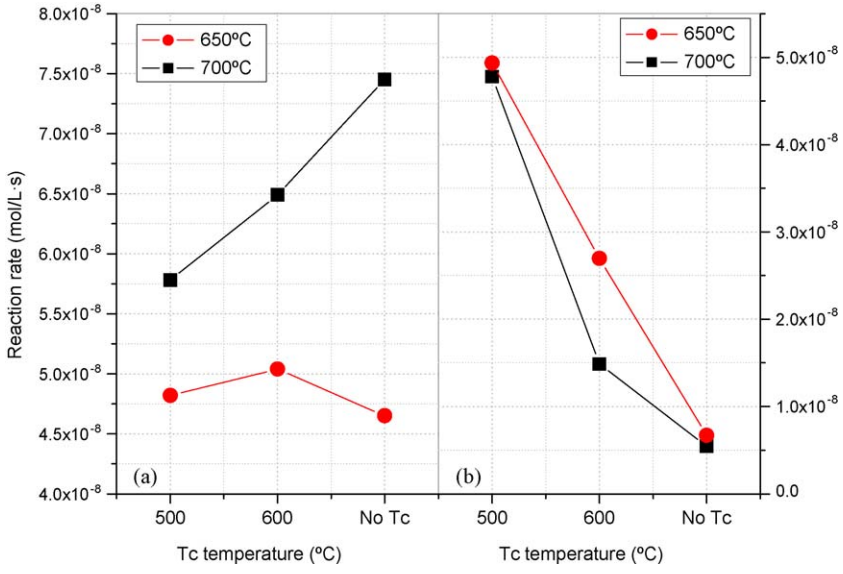

Fig. 10. Evolution of reaction rate for (a) liquid phase phenol and (b) toluene gas phase degradation reactions.

4. Conclusions

The partial calcination in nitrogen at temperatures above 500 °C seems to stabilize the surface sulfates from the impregnation procedure. This stabilization appears more evident for samples calcined at 650 °C. The presence of this sulfur vestige at the surface induces important changes in the crystalline structure. Though all samples show anatase phase structure, the strain generated by the presence of sulfur surface species is clearly evidenced from XRD and Raman spectroscopy. The strain has two main components derived from the presence of oxygen sub-surface defects as well as surface (sulfate-related) species. The first dominates air calcined samples while sulfates make an important contribution if the calcination is run under nitrogen. Moreover in samples partially calcined in nitrogen this structural and/or surface stress could be related with the existence of sulfate residues linked at the surface. The presence of sulfates plainly affects the photocatalytic activity for phenol degradation reaction. Thus, the defective structure at the outer layers plays a detrimental influence for such reaction. The optimal situation is shown by the samples calcined in air. The effect of sulfate during calcination provides the stabilization of the surface and the structure, leading to the best situation for this reaction when the amount of sulfate is almost negligible.

On the contrary, the existence of a small amount of surface sulfate residues positively affects to the photocatalytic performance for toluene degradation in the gas phase. For such reaction, the sulfur species would enhance the surface acidity. Thus, the best conversion rates are obtained for the samples partially calcined in nitrogen from T_c = 500 °C, for which the amount of sulfates are slightly higher. The existence of a certain surface defective structure is balanced in this case for the enhancement in the surface acidity leading to the contrary tendency for toluene photodegradation reaction.

Acknowledgments

Financial support by Junta de Andalucía (P.A.I.D.I. group FQM181 annual funding and Excellence Project P06-FQM-1406) and CICYT (CTQ2007-60480/BQI and CTQ2008-05961-C02-01) are acknowledged. A.K. thanks the CSIC for a I3P Postdoctoral grant.

References

[1] G. Colón, C. Belver, M. Fernández-García, in: M. Fernández-García, J.A. Rodríguez (Eds.), Synthesis, Properties and Application of Oxide Nanoparticles, Wiley, USA, 2007, , ISBN: 978-0-471-72405-6, Chapter 17.
[2] O. Carp, C.L. Huisman, A. Reller, Prog. Solid State Chem. 32 (2004) 33.
[3] H.Y. Zang, G.X. Xiong, W.S. Yang, X.Z. Fu, Acta Phys. Chim. Sinica 17 (2001) 273.
[4] Y.T. Kwon, K.Y. Song, W.I. Lee, G.J. Choi, Y.R. Do, J. Catal. 191 (2000) 192.
[5] A. Fuerte, M.D. Hernandez-Alonso, A.J. Maira, A. Martinez-Arias, M. Fernandez-García, J.C. Conesa, J. Soria, G. Munuera, J. Catal. 212 (2002) 1.
[6] A. Kubacka, M. Fernández-García, G. Colón, J. Catal. 254 (2008) 272.
[7] D.S. Muggli, L. Ding, Appl. Catal. B: Environ. 32 (2001) 181.
[8] W.Y. Su, X.Z. Fu, K.M. Wei, Acta Phys. Chim. Sinica 17 (2001) 28.
[9] X.Z. Fu, W.A. Zeltner, Q. Yang, M.A. Anderson, J. Catal. 168 (1997) 482.
[10] X. Deng, Y. Yue, Z. Gao, Appl. Catal. B: Environ 39 (2002) 135.
[11] G. Munuera, A.R. González-Elipe, V. Rives-Arnau, J.A. Navío, P. Malet, J. Soria, J.C. Conesa, J. Sanz, Stud. Surf. Sci. Catal. 21 (1985) 113.
[12] G. Colón, M.C. Hidalgo, J.A. Navío, Appl. Catal. B: Environ. 45 (2003) 39.
[13] G. Colón, M.C. Hidalgo, G. Munuera, I. Ferino, M.G. Cutrufello, J.A. Navío, Appl. Catal. B: Environ. 63 (2006) 45.
[14] J.A. Rengifo-Herrera, E. Mielczarski, J. Mielczarski, N.C. Castillo, J. Kiwi, C. Pulgarin, Appl. Catal. 84 (2008) 448.
[15] L. Castro, P. Reyes, C. Montes, J. Sol Gel Sci. Technol. 25 (2002) 159.
[16] X. Yang, F.C. Jentoft, R.E. Jentoft, F. Girgsdies, T. Ressler, Catal. Lett. 81 (2002) 25.
[17] G.K. Williamson, W.H. Hall, Acta Metall. 1 (1953) 22.
[18] D. Briggs, M.P. Seah, Practical Surface Analysis by Auger and X-ray Photoemission Spectroscopies, John Wiley, New York, 1983.
[19] A.J. Maira, K.L. Yeung, J. Soria, J.M. Coronado, C. Belver, C.Y. Lee, V. Augugliaro, Appl. Catal. B: Environ. 29 (2001) 327.
[20] T. Yamaguchi, Appl. Catal. 61 (1990) 1.
[21] G. Busca, G. Ramis, J.M. Gallardo Amores, V. Sanchez Escribano, P. Piaggio, J. Chem. Soc., Faraday Trans. 90 (1994) 3181.
[22] M.H. Lee, B.C. Choi, J. Am. Ceram. Soc. 74 (1991) 2309.
[23] Y.S. Bobovich, M.Y. Tsenter, Opt. Spectrosc. 53 (1982) 332.
[24] J.C. Parker, R.W. Siegel, J. Mater. Res. 5 (1990) 1246.
[25] H.C. Choi, Y.M. Jung, S.B. Kim, Vib. Spectrosc. 37 (2005) 33.
[26] M. Fernández-García, A. Martínez-Arias, J.C. Hanson, J.A. Rodriguez, Chem. Rev. 104 (2004) 4063.
[27] T. Ohsaka, F. Izumi, Y. Fujiki, J. Raman Spectrosc. 7 (1978) 321.
[28] X.Z. Fu, W.A. Zeltner, Q. Yang, M.A. Anderson, J. Catal. 168 (1997) 428.
[29] E. Barraud, F. Bosc, N. Keller, V. Keller, Chem. Lett. 34 (2005) 336.
[30] M.A. Fox, M.T. Dulay, Chem. Rev. 93 (1993) 341.
[31] C.S. Turchi, D.F. Ollis, J. Catal. 122 (1990) 178.
[32] A. Yamakata, T. Ishibashi, H. Onishi, Chem. Phys. Lett. 376 (2003) 576.
[33] I.A. Shkrob, M.C. Sauer Jr., D. Gosztola, J. Phys. Chem. B 108 (2004) 12512.